

LA-UR-20-24874 (Accepted Manuscript)

First Direct Observations of Propagation of Discrete Chorus Elements From the Equatorial Source to Higher Latitudes, Using the Van Allen Probes and Arase Satellites

Colpitts, C. A.; Miyoshi, Yoshizumi; Kasahara, Y.; Wygant, J. R.; Cattell, C.; Breneman, Aaron; Kletzing, C. A.; Cunningham, Gregory Scott; Delzanno, Gian Luca; Hikishima, M.; Matsuda, S.; Katoh, Y.; Ripoll, J. F.; Shinohara, I.; Matsuoka, A.

Provided by the author(s) and the Los Alamos National Laboratory (2020-12-18).

To be published in: Journal of Geophysical Research: Space Physics

DOI to publisher's version: 10.1029/2020JA028315

Permalink to record: <http://permalink.lanl.gov/object/view?what=info:lanl-repo/lareport/LA-UR-20-24874>

Disclaimer:

Los Alamos National Laboratory, an affirmative action/equal opportunity employer, is operated by Triad National Security, LLC for the National Nuclear Security Administration of U.S. Department of Energy under contract 89233218CNA000001. By approving this article, the publisher recognizes that the U.S. Government retains nonexclusive, royalty-free license to publish or reproduce the published form of this contribution, or to allow others to do so, for U.S. Government purposes. Los Alamos National Laboratory requests that the publisher identify this article as work performed under the auspices of the U.S. Department of Energy. Los Alamos National Laboratory strongly supports academic freedom and a researcher's right to publish; as an institution, however, the Laboratory does not endorse the viewpoint of a publication or guarantee its technical correctness.



First direct observations of propagation of discrete chorus elements from the equatorial source to higher latitudes, using the Van Allen Probes and Arase satellites

Chris Colpitts¹, Yoshizumi Miyoshi², Yoshiya Kasahara³, Gian Luca Delzanno⁴, John R Wygant¹, Cynthia A Cattell¹, Aaron Breneman¹, Craig Kletzing⁵, Greg Cunningham⁴, Mitsuru Hikishima⁶, Shoya Matsuda⁶, Yuto Katoh⁷, Jean-Francois Ripoll⁸, Iku Shinohara⁶, Ayako Matsuoka⁹

(1) University of Minnesota Twin Cities, Minneapolis, MN, (2) Nagoya University, Nagoya, Japan, (3) Kanazawa University, Kanazawa, Japan, (4) Los Alamos National Laboratory, Los Alamos NM, (5) University of Iowa, Iowa City, IA, (6) ISAS/JAXA, Sagamihara, Japan, (7) Tohoku University, Sendai, Japan, (8) CEA, DAM, DIF, F-91297 Arpajon, France; UPS, CEA, LMCE, 91680 Bruyères-le-Châtel, France, (9) Kyoto University, Kyoto, Japan

This is the author manuscript accepted for publication and has undergone full peer review but has not been through the copyediting, typesetting, pagination and proofreading process, which may lead to differences between this version and the [Version of Record](#). Please cite this article as doi: [10.1029/2020JA028315](https://doi.org/10.1029/2020JA028315)

Abstract

Whistler mode chorus waves have recently been established as the most likely candidate for scattering relativistic electrons to produce the electron microbursts observed by low altitude satellites and balloons. These waves would have to propagate from the equatorial source region to significantly higher magnetic latitude in order to scatter electrons of these relativistic energies. This theoretically proposed propagation has never been directly observed. We present the first direct observations of the same discrete rising tone chorus elements propagating from a near equatorial (Van Allen Probes) to an off-equatorial (Arase) satellite. The chorus is observed first on the more equatorial satellite, and is found to be more oblique and significantly attenuated at the off-equatorial satellite. This is consistent with the prevailing theory of chorus propagation, and with the idea that chorus must propagate from the equatorial source region to higher latitudes. Ray tracing of chorus at the observed frequencies confirms that these elements could be generated parallel to the field at the equator, and propagate through the medium unducted to Van Allen Probes A and then to Arase with the observed time delay, and have the observed obliquity and intensity at each satellite.

Introduction/Background

Electromagnetic whistler mode waves have long been among the most commonly observed and studied space plasma emissions (see e.g. Burtis and Helliwell, 1969; Taylor and Gurnett, 1968). Within the Earth's magnetosphere, whistler mode waves are typically observed as either broadband hiss found inside the plasmasphere and in plumes (Thorne et al, 1973; Meredith et al.,

2006, Malaspina et al., 2016 and 2018; Hartley et al., 2018), or discrete emissions observed outside the plasmopause known as chorus waves (Tsurutani and Smith, 1977; Li et al, 2009 and 2016), occasionally at very large amplitudes in the radiation belts (Cattell et al., 2008 and 2012). These chorus waves typically (but not always (Kurita et al., 2012)) occur in two bands separated by a gap at half the equatorial electron cyclotron frequency f_{ce} , and are often observed as discrete rising (increasing in frequency with time) or falling (decreasing) tones lasting a few tenths of a second. Chorus waves directly impact magnetospheric particles in several distinct ways. These waves can be both a source and a loss mechanism for radiation belt particles (Horne and Thorne, 1998; Myoshi et al., 2003; Meredith et al., 2003; Turner et al., 2013, Reeves et al., 2013; Thorne et al., 2013). They are also believed to be responsible for diffuse and pulsating aurora (Nishimura et al., 2010; Thorne et al., 2010; Miyoshi et al., 2015a; Kasahara et al., 2018a; Ozaki et al., 2019; Agapitov et al., 2018; Hosokawa et al., 2020), and possibly for plasmaspheric hiss as well (Santolik et al., 2006; Bortnik et al., 2008 and 2009; Meredith et al., 2013), although there are alternative theories (e.g. Falkowski et al. 2017, Hartley et al. 2019). Additional studies and current open research questions related to chorus waves can be found in Ripoll et al. (2020) and references therein.

In addition, whistler mode chorus waves have been studied in association with electron microburst precipitation. Microbursts are precipitation events of keV-MeV electrons observed to be highly localized and lasting 10s to 100s of ms (Anderson and Milton, 1964; Blake et al., 1996). They are observed at lower altitude but on the same field lines as the outer radiation belt most often during the main phase and early recovery phase of geomagnetic storms, and may be a significant loss mechanism for outer belt electrons during stormtime (O'Brien et al., 2004;

Lorentzen et al., 2001a). Whistler mode chorus waves were first proposed as the scattering mechanism for these precipitating electrons due to the similar spatial location and temporal characteristics of the observed chorus and microbursts (Oliven and Gurnett, 1968; Rosenberg et al., 1971 and 1981; Nakamura, 2000; Lorentzen et al., 2001a and 2001b, Kersten et al., 2001, Breneman et al., 2007; Mozer et al., 2018). Recently this relationship was directly shown by Breneman et al. (2017) for the first time through observations of chorus emissions on Van Allen Probes A and microburst precipitation on the FIREBIRD II CubeSat (Spence et al., 2012; Crew et al., 2016; Johnson et al., 2020).

The mechanism for chorus waves to scatter electrons which then precipitate into the ionosphere as electron microbursts has also been studied extensively. The most promising mechanism is scattering into the bounce loss cone via first order cyclotron resonance (Horne and Thorne, 2003; Lorenzen et al., 2001b; Breneman et al., 2017). However, this mechanism cannot act on relativistic electrons within the presumed equatorial chorus source region. The resonance energy is too low in this region, but at higher latitudes along a given field line the field line convergence increases the magnetic field strength and therefore the resonant energy. The chorus waves would thus have to propagate to higher magnetic latitudes before interacting with and scattering these electrons (Miyoshi et al., 2015b).

Chorus waves are generated near the magnetic equator (LeDocq et al., 1998), where the Earth's magnetic field B is minimized, and the field lines are straight relative to higher latitudes. This combination enhances the ability of the electron distribution to become sufficiently anisotropic for wave growth rates high enough to generate the observed chorus (Omura, Katoh and Summers

2008), and allows the coherent resonance necessary to produce the rising tones. Chorus is observed throughout the inner magnetosphere outside the plasmapause, and the theory of the propagation of these emissions is well established (e.g. Santolik et al., 2009; Katoh et al., 2014; Turner et al. 2017). The emissions propagate away from the equator in both directions along magnetic field lines, though depending on conditions they can refract to move slightly radially inward (or even outward) transverse to the field as they propagate (e.g. Turner et al. 2017).

Understanding how chorus wave properties change as they propagate away from the equator is critical because the minimum cyclotron resonance energy is a function of wave normal angle. Therefore, the range of electron energies that can interact with chorus waves at a given location depends on this wave normal angle. These properties are a function of L, MLT, magnetic latitude, and geomagnetic activity level (Agapitov et al., 2015). This affects both the growth of chorus waves and the variation (lifetime and energization rates) of energetic electron outer belt flux. For example, relativistic electron microbursts observed on FIREBIRD have been linked to off-equatorial scattering from highly oblique chorus waves at latitudes > 20 deg (Breneman et al., 2017).

Theory and ray tracing studies show the waves tend to become more oblique and to decrease in amplitude as they propagate to higher magnetic latitudes (amplitude decrease arises from a number of mechanisms, chiefly a change in wave normal angle and geometrical spread at low latitudes, cyclotron damping at mid-latitudes and Landau damping at high latitudes) (Bortnik et al., 2007a and 2007b; Santolik et al., 2009 and 2010; Breuillard et al., 2012 and 2013; Chen et al., 2013; Katoh, 2014). Statistical observational studies (Li et al., 2011, 2013 and 2016;

Agapitov et al., 2013 and 2015) mostly support these characteristics of chorus propagation, but observationally the majority of chorus power at 10-15 degrees latitude is more field-aligned and less attenuated than simple, unducted ray tracing would suggest, and the bulk of chorus wave power doesn't become significantly oblique until 30 degrees latitude (Santolik et al., 2014). This tendency towards remaining field-aligned may be due to selective growth, whereby more field-aligned waves are enhanced as they resonate with off-equatorial electrons relative to less field-aligned waves. The existence of field-aligned density ducts would also tend to keep wave normal angles field-aligned, and in fact ducted propagation is required to replicate these observations of field aligned chorus at high latitudes (Hanzelka and Santolik, 2019). Evidence of such field-aligned ducts in this region has been observed (see e.g. Yearby et al., 2011). However, given the ubiquity of chorus observations at these higher latitudes, direct observation and confirmation of chorus waves propagating unducted to higher latitudes would significantly enhance our understanding of chorus propagation. In order to understand how these observed chorus distributions arise it is vital to directly study the evolution of chorus amplitudes and wave normal angles with multi-point measurements.

For the proposed mechanism of chorus waves causing electron microburst precipitation through first order cyclotron resonance, the chorus waves would often need to propagate from the near-equatorial source to higher magnetic latitude. This theoretical propagation of chorus has never been directly confirmed through observations of discrete chorus elements as they propagate from their equatorial source to higher latitudes. The launch of the Exploration of energization and Radiation in Geospace (ERG, or Arase) satellite (Miyoshi et al., 2018a) on December 20, 2016 added a radiation belt probe with an orbit at higher inclination (31 degrees). Arase thus traverses

the magnetic latitudes at which this wave-particle interaction is predicted to occur, and allows us to look for chorus wave propagation from a near-equatorial satellite such as Van Allen Probes to these higher latitudes.

In this paper, we present the first observations of individual discrete rising tone chorus elements propagating from a satellite near the equatorial source region to a satellite at significantly higher magnetic latitude. In Section 2 we show the event observations, in Section 3 the ray tracing analysis, and in Section 4 we present our conclusions.

Data Presentation – Satellite Observations

On August 21, 2017 from 0135-0203 UT, there was a close (L separated by $<1 R_E$ and MLT separated by <1 hour) magnetic conjunction between the Van Allen Probes A (RBSP) and Arase satellites. In anticipation of this, the RBSP and Arase teams collected burst waveform data throughout the time interval of the conjunction. The closest approach between the two satellites was 4368 km, but the minimum L-shell separation (determined from McIlwain L-shell and IGRF model) was 0.028 L and the minimum MLT difference was 0.178 hours. Therefore, almost the entire separation was in magnetic latitude, which can be seen in Figure 1, with the minimum separation in the GSM xy-plane (transverse separation) being 1080 km. It is notable that the total spacecraft separation (>4368 km) is considerably larger than the source scale for whistler wave packets, ~ 500 -800 km (Agapitov et al., 2017 and 2018), requiring propagation for the waves to be observed on both spacecraft, but the transverse separation is comparable to this scale size.

Figure 1 shows the locations of the RBSP A (red) and Arase (blue) satellites from 0100-0200 UT on August 21, 2017 in GSM coordinates. The first panel shows GSM Y versus GSM X, and one can see that the two satellites are nearly co-located in these coordinates (i.e. in MLT and L-shell) from 0145-0200. The second and third panels show GSM Z vs GSM Y and GSM X respectively, and show a separation in GSM Z, i.e. a separation in magnetic latitude.

At this time, the location of the two satellites in the equatorial plane is roughly 16.5 MLT and L-shell 3.5-4.0. This corresponds to the duskside region, near the inner edge of the outer radiation belt, outside the plasmopause. This region is outside of the peak location of chorus observations, which is on the dawn and dayside, particularly at times of low to moderate geomagnetic activity, but well within the region of observed chorus waves (Li et al, 2016, Tyler et al., 2019a and 2019b). Latitudinally, at 0145 UT the two satellites are at ~12 degrees MLAT (RBSP A) and ~21 degrees MLAT (Arase). Both statistical observations (Agapitov et al., 2013 and 2015, Santolik et al., 2014) and ray tracing studies (Chen et al., 2013, Katoh 2014) indicate that, at these latitudes, chorus elements generated in the presumed equatorial source region with parallel wave normal angle are likely to become increasingly oblique and thus more electrostatic.

This conjunction occurred during a period of mild geomagnetic activity. An overview of this period is shown in Figure 2, with a vertical dashed line indicating the time of the observations shown in Figures 3 and 4. Figure 2 (a) and (b) show the geomagnetic conditions during the time interval of the conjunction. The top panel shows the Auroral Electrojet (AE) index, and the second panel shows the SYM/H index, both at 1 minute resolution from the WDC Kyoto database. The AE index varies from ~150-400 nT, with signatures of two small substorms at

0046 and 0132. The SYM/H index rises gradually from -23 to -15 nT, consistent with mild geomagnetic activity. Figure 2 (e) shows the electron density (computed from the Upper Hybrid line) in cm^{-3} observed at Van Allen Probes A. At ~0155 UT the spacecraft crosses the eroded plasmopause, and Arase crosses this same feature at ~0210 (after the time of the plot and thus not shown). During the time of the observations (~0145 UT), both spacecraft are near the edge of the plasmasphere, just outside the plasmopause, with densities of $\sim 60 \text{ cm}^{-3}$ (Van Allen) and $\sim 100 \text{ cm}^{-3}$ (Arase).

During this time Van Allen Probes A observed relatively weak wave activity in several wavemodes. Figure 2 (c) and (d) show spectrograms of the wave electric and magnetic field from the EMFISIS instrument (Kletzing et al., 2013) on RBSP A. The dominant wave mode during this time is a broadband signal from ~100-2500 Hz. At lower frequencies 5-10 Hz, we can see another mode emerge in the electric field late in the interval 0155-0200. The Power Spectral Density, shown in color scale, of all wavemodes shows that these waves are low amplitude, consistent with the weak geomagnetic activity seen in the top two panels.

At higher frequencies 2500-8000 Hz, we can see whistler mode chorus waves, most notably in the electric field. Specifically, from ~0130-0200 there is wave power in this mode in the electric field comparable to that in the other wave modes, while in the magnetic field there is only a small amount of wave power visible at this time in this color scale at ~0145. Despite this weak signal, this is the series of chorus elements that were observed to propagate from Van Allen Probes A to the location of Arase.

Figure 3 shows 5800-7300 Hz spectrograms of the burst waveform data taken by the Van Allen Probes A Electric Field and Waves (EFW) instrument (Wygant et al., 2013) and the Arase Wave Form Capture of the Plasma Wave Experiment (PWE) (Kasahara et al., 2018b; Matsuda et al., 2018) during a 30 second interval within this conjunction (spectrograms are generated using $df = 32$ Hz, and $dt = 7.8125$ ms for Arase, 62.5 ms for RBSP). Electric field measurements are shown in panels (a) and (c), magnetic field data in panels (b) and (d). A sequence of discrete rising tone chorus elements is observed on both spacecraft, with several of the same elements evident in all four spectrograms. These are lower band chorus elements, with frequencies 6300-7100 Hz = 0.40-0.45 f_{ce} as calculated from the RBSP magnetic field measurements. At this time $f_{ce}/2$ is ~7900 Hz (above the plot range) and does not change significantly during this time period.

Figure 4 shows these same magnetic spectrograms again, zoomed in to 01:45:36-01:45:46, with the power spectral density in panels (a) (RBSP A) and (c) (Arase). A vertical dashed white line at around 01:45:38.10 indicates the time of the first rising tone chorus element's arrival at RBSP A from the equatorial source. This same chorus riser can be seen to arrive at Arase around 01:45:38.30, or about ~0.20 seconds later. The second chorus riser seen at around 01:45:38.40 on RBSP A is then observed with the same ~0.20 second delay at Arase. This same delay is also observed for the next 3 riser tone elements. There is an absolute maximum timing uncertainty of ~0.10 seconds due to satellite operations, but the actual error is typically far less. The observed 0.20 second delay in the arrival of the chorus risers is thus significant, and demonstrates that the waves arrive at Arase later even with the maximum timing uncertainty, so that we can compare this result with theory and ray tracing results.

The wave normal angles are plotted in color scale from 0 to 90 degrees in panels (b) (RBSP A) and (d) (Arase). The ambient magnetic field is derived from the EMFISIS fluxgate magnetometers on RBSP (Kletzing et al., 2012) and from the MGF instrument on Arase (Matsuoka et al., 2018). For these panels we remove all data beneath a given wave power threshold (.01 pT²/Hz for RBSP A and .0005 pT²/Hz for Arase) to isolate the rising tone elements. The magnetic field power is observed to be lower at the location of Arase than the location of RBSP A. Calculating the wave intensity from the spectral data by integrating over the frequencies 6000-7000 Hz gives intensities of ~2.5-5.0 pT at RBSP A and ~1.2-1.5 pT at Arase. These values represent extremely weak chorus and are consistent with chorus waves propagating from a near-equatorial source, first to RBSP A and then to Arase (Breuillard et al., 2013). The observation of low magnetic field power relative to the electric field power seen in Figure 3 is consistent with the large wave-normal angle of these chorus elements shown in Figure 4 (Artemyev et al., 2016; Albert, 2017).

Wave normal angles are determined assuming a plane wave, by calculating the angle between the direction of minimum variance in the search coil magnetometer data (calculated from the complex off-diagonal elements of the spectral matrix) and the direction of the background magnetic field (Means et al., 1972; Santolik et al., 2003). The measured wave normal angle at RBSP A is ~50-60 degrees, while at Arase the waves have become significantly more oblique, with a wave normal angle of ~70-80 degrees. We can see from this figure that the waves (i.e. all 5 risers seen in Figure 4) are significantly more oblique (red) at Arase than at Van Allen Probes. However, due to the low signal-to-noise ratio of these Arase wave observations, the wave normal angle calculation is uncertain and should be considered a rough estimate. It is informative to

look also at the spread in wave normal angle observations at the two satellites to see the degree of uncertainty. Figure 5 shows a histogram of the WNA calculated at each frequency and time bin shown in Figure 4. The Van Allen Probes measurements show a relatively narrow peak around ~45-55 degrees. While the spread in the values of WNA for Arase is broader due to the weaker signals, the occurrence rate clearly peaks at a more oblique angle than that observed at Van Allen Probes A, around ~75-85 degrees.

These wave normal angles are consistent with the theory of propagation from a near-equatorial source, becoming more oblique as the waves propagate to higher latitudes. (Although, as will be shown in Section 4, to reach these high wave normal angles at these locations, the waves at the equatorial source would have to have a significant wave normal angle.) These different measured wave normal angles observed at the two satellites are the same for all five of the rising tone chorus elements. In addition, Figure 4 (e) shows the parallel Poynting flux of the chorus waves observed by Van Allen probes, with positive flux being northward. The waves show a clear tendency towards northward propagation, though there is some spread in the direction of the Poynting vector due to low signal-to-noise ratio. The Poynting vector of the Arase observations (not shown) exhibits even more spread but also shows a tendency towards northward propagation. This is also consistent with propagation from a near-equatorial source, first to the location of the Van Allen Probes satellite and then on to the location of Arase.

Ray Tracing Analysis

These observations appear to be consistent with the theory of chorus wave generation and propagation, and with previous ray tracing studies. We can confirm this by launching a simulated chorus mode wave at the presumed source location near the geomagnetic equator and tracing the ray to see if it reaches the spacecraft locations with the observed characteristics. We have performed several ray-tracing simulations to study the propagation of chorus waves between the two spacecraft. The details of the simulations are discussed in the Appendix.

An example ray tracing simulation is shown in Figure 6, which shows the trajectory of 30 main rays initialized with 18° wave normal angle and 6.8 kHz frequency (red dashed lines represent the dipole magnetic field lines). The plasma density model given by Eq. (1) is used here. The solid (dashed) black line highlights the trajectory of the first (last) ray, $x_0 = 3.9R_E$ ($x_0 = 4.2R_E$). The red diamond (square) labels Van Allen Probes (Arase). One can notice the focusing of the rays primarily due to the magnetic field inhomogeneity. In this particular instance, only 4 rays intercept both spacecraft when $\delta = 0.005$ is used in Eq. (3). Note that δ represents a finite area near each spacecraft which we use to determine when the waves hit the spacecraft.

Results from our simulation campaign varying the frequency of the rays and the minimum distance from each spacecraft δ are summarized in Table 1. The majority of the runs are also performed with the plasma density model given by Eq. (1). For the 6.5 kHz frequency, δ is changed between 0.002 and 0.1. At $\delta = 0.002$, only one ray intercepts both spacecraft, starting at $x_0 = 4$ with wave normal angle of 23° . For $\delta = 0.01$, 48 rays intercept both spacecraft giving a larger spread in the results in the data reported in Table 1. $\delta = 0.005$ is a compromise between having too few rays meeting both spacecraft and a larger spread in the wave properties: it yields

10 rays intercepting both spacecraft. The initial wave normal angles range between 22° and 25° . The propagation time from Van Allen Probes to Arase is between 0.13-0.14 s. This is consistent with the observations, and indeed provides confirmation that the timing uncertainty is considerably less than 100 ms at the time of the observations. The wave normal angle at Van Allen Probes ranges between 56° and 59° , with a mean of 57° . The spread in wave normal angle at Arase is lower, due to focusing of the rays, ranging from 72.8° to 73.6° with 73.2° mean. Finally, the ratio of the magnetic field wave amplitude at Van Allen Probes relative to Arase ranges between 1.7 and 2.0, with 1.9 mean. The fourth and fifth columns of Table 1 report data for 6.8 kHz and 7.1 kHz ($\delta = 0.005$) with the same format. The initial wave normal angle is lower, between 17° and 19° for 6.8 kHz and 12° and 14° for 7.1 kHz. The mean wave normal angle at Van Allen Probes is also lower for these higher frequencies, with 54° mean (53° - 56° range) for 6.8 kHz and 52° mean (51° - 53° range) for 7.1 kHz. At Arase, the mean wave normal angle is 72° (6.8 kHz) and 71° (7.1 kHz) with less than 1° in spread in both cases. The ratio of magnetic field wave amplitude at Van Allen Probes relative to Arase is approximately 2.

The last column of Table 1 shows data for 6.8 kHz ($\delta = 0.005$) obtained with the density model of Eq. (4), i.e. for an L^{-4} dependence of the density. Relative to data obtained for the model given by Eq. (1) (L^{-5} dependence of the density, fifth column of Table 1), one can see that the initial wave normal angle is a bit smaller (12° - 15°) but the range of wave normal angles at Van Allen Probes and Arase are essentially the same. The magnetic field wave amplitude ratio is about 10% higher, but still in good agreement. This indicates that the results presented in this paper are not too sensitive to the density model adopted, probably because of the relatively short separation between the two spacecraft.

The data reported in Table 1 shows that chorus waves initialized in the equatorial plane must have a finite, frequency-dependent, wave normal angle to meet both spacecraft. Since chorus waves generated by the whistler instability are predominantly field-aligned, this suggests that the wave generation process occurred for $z_0 < 0$. Furthermore, over the frequency range of interest, our model predicts a range of wave normal angles 51° - 59° at Van Allen Probes and 71° - 74° at Arase with a time delay of 0.128-0.136 seconds and a wave-amplitude ratio between 1.7 and 2.5. Note that in these studies the wave amplitudes change due to changes in wave normal angle and geometric focusing/defocusing due to gradients. We are not accounting for wave damping but the good agreement with the observations suggests that damping effects should be small.

These results are in excellent agreement with the observations reported above, confirming that the propagation of these chorus elements between the two spacecraft can be replicated with unducted chorus wave propagation. This result establishes that chorus can also propagate unducted to higher latitudes, becoming significantly attenuated and oblique; however it is still consistent with the theory that for chorus to propagate to high latitudes while remaining field-aligned and without significant attenuation as is often observed, ducted propagation would be required.

Conclusions and Future Work

The recent confirmation of the relationship between whistler mode chorus waves and electron microburst precipitation by Breneman et al. (2017) further demonstrates the importance of

experimentally verifying the propagation of chorus from the equatorial source to higher magnetic latitudes, as required to scatter relativistic electrons. Theoretical models for the generation of relativistic electron microbursts via chorus have suggested this propagation, which is supported by a number of ray tracing and statistical studies. However, observations reveal chorus waves at higher latitudes tend to be more field-aligned and less attenuated than would be suggested by simple ray tracing. Additionally, the limited latitudinal range of existing satellites has until now precluded the direct observation of this propagation (Horne and Thorne, 2003, Miyoshi et al., 2015b). The launch of the Arase satellite with an orbit covering these higher magnetic latitudes allows us to directly observe chorus wave propagation.

We present the first direct observations of the same discrete rising tone chorus elements propagating from a near equatorial (Van Allen Probes) to an off-equatorial (Arase) satellite. The chorus is observed first on the equatorial satellite, and then on the higher latitude one where the waves are found to have more oblique wave normal angles and significantly reduced amplitudes. This is consistent with the accepted theory of chorus propagation, and with the idea that chorus must propagate from the equatorial source region to higher latitudes in order to generate relativistic electron microbursts. Performing ray tracing of chorus at these frequencies confirms that these elements could be generated with wave angles parallel or quasi-parallel to the field at the near-equatorial source, and propagate unducted to Van Allen Probes A and then to Arase, with the observed time delay, amplitude and obliquity at each satellite.

This result is the first direct confirmation of the theoretically proposed propagation of whistler mode chorus waves to high latitudes, where they are believed to be the responsible mechanism

for generating relativistic electron microbursts. This result will be further reinforced by other observations and studies. We have many additional conjunctions between Arase and one of the Van Allen Probe satellites between 2017 and 2019 for which we collected burst mode waveform data on both satellites. We will perform additional case studies and statistical studies of chorus mode wave propagation using these conjunctions to provide further confirmation of these results. In addition, we have data from other conjunctions between Van Allen Probes in the radiation belts and the Firebird II CubeSats in low earth orbit, with which we will perform a statistical study of the chorus waves observed on RBSP in the equatorial source region and the microbursts observed at LEO (Johnson et al., 2020). Together, these studies will provide a complete picture of the propagation of chorus waves in the inner magnetosphere and the generation of electron microbursts by these waves.

Appendix

The ray-tracing code closely follows the one developed by Horne (1989), where rays propagate in an Earth-centric, Cartesian reference frame (x, y, z) , using the cold-plasma approximation. We use a standard dipole model for the Earth's magnetic field, which is a good approximation for the relative low L shells ($L \sim 4$) considered here. We use a cold-plasma model to characterize the waves with the background plasma density given by

$$n_0 = \frac{6.045 \cdot 10^4}{L^5} [cm^{-3}] \quad (1).$$

The constant in Eq. (1) is chosen to match the density of 67 cm^{-3} at the position of Van Allen Probes ($L=3.9$) for the case of interest, while the L^{-5} dependence is determined from a fit to the total electron density data obtained by the Van Allen Probes' EMFISIS instrument using

measurements of the upper-hybrid line on Aug. 21st 2017 near 1:45 UT (See Figure A1). To compute the change in wave amplitude as the ray propagates, we initialize a triplet of rays at a given spatial location (x_0, y_0, z_0) : the main ray is characterized by (α_0, φ_0) , i.e. (polar) wave normal angle and azimuthal wave normal angle, while the two auxiliary rays are characterized by $(\alpha_0 + 0.005 \text{ rad}, \varphi_0)$ and $(\alpha_0 + 0.01 \text{ rad}, \varphi_0 + 0.005 \text{ rad})$. As the triplet propagates, we use these three rays to define the differential (triangular) area dA perpendicular to the direction of motion of the main ray, at each point of the trajectory. Since power is conserved along the ray trajectory, i.e.

$$\text{Re}(SdA) = \text{Re}(S_0dA_0), \quad (2)$$

where Re represents the real part and S the Poynting flux, we can use cold-plasma theory to recast Eq. (2) as an equation for the amplitude of the wave electric or magnetic field (relative to the initial amplitude) along the ray trajectory.

For each value of frequency and initial wave normal angle, 30 rays are initialized in the equatorial plane, with position $(x_0, 0, 0)$ and x_0 uniformly spaced in the interval $(3.9 - 4.2) \cdot R_E$ (where R_E is the Earth radius). The wave normal angle is treated parametrically in 1° increments. We do not model the longitudinal separation between the two spacecraft, which as discussed earlier in the description of Figure 1 is very small, ~ 1000 km (interestingly, this distance is comparable to than the source scale for whistler wave packets, ~ 500 - 800 km, reported by Agapitov et al., 2017 and 2018). The main rays are initialized with zero azimuthal angle, $\varphi_0 = 0$, and wave vector $k_y = 0$, finite k_x and k_z . Hence, the main rays move in the $y=0$ plane. The spacecraft positions are $x_{\text{VAP}} = 3.65R_E$, $z_{\text{VAP}} = 0.77R_E$ and $x_{\text{ARASE}} = 3.05R_E$, $z_{\text{ARASE}} = 1.15R_E$. A ray is assumed to intercept Van Allen Probes when the following condition is satisfied:

$$\left| \frac{x - x_{VAP}}{R_E} \right| < \delta, \left| \frac{z - z_{VAP}}{R_E} \right| < \delta, \quad (3)$$

where δ is also treated as a parameter, and similarly for Arase. δ is simply used to define a small area near each spacecraft which we use to identify if the waves hit the spacecraft or not. It reflects the fact that with finite resolution and specific initial conditions the waves might miss the exact location of the spacecraft.

Since the background density model is critical for the propagation of the waves, we have performed another set of simulations with a different density model given by:

$$n_0 = \frac{1.55 \cdot 10^4}{L^4} [cm^{-3}] \quad (4).$$

A L^{-4} dependence of the cold plasma density has been used in other studies of resonant wave-particle interactions with chorus waves (Summers et al., 2007) and has been shown to be a good fit of CRRES data in the trough (Sheeley et al., 2001).

Acknowledgements

This work was supported by RBSP-EFW funding provided by JHU/APL contract 922613, under NASA's prime contract NAS5-01072, and by NASA grant 80NSSC19K0842. Research was supported by the International Space Science Institute's (ISSI) International Teams program. Van Allen Probes data used in this paper can be found in the EFW (<http://www.space.umn.edu/rbspew-data/>) and EMFISIS (<http://emfisis.physics.uiowa.edu/data/index>) archives. Science data of the ERG (Arase) satellite were obtained from the ERG Science Center operated by ISAS/JAXA and ISEE/Nagoya University (<https://ergsc.isee.nagoya-u.ac.jp/index.shtml.en>, Miyoshi et al., 2018b). In the present study, we used level 2 PWE/WFC waveform v00.01 data, level 2 MGF 8 s v03.03 data and level 2 definitive orbit v02 data. Part of this work was done at the ERG-Science Center operated by ISAS/JAXA and ISEE/Nagoya University. GLD wishes to thank Pat Colestock for stimulating discussions. GLD and GSC were supported by the Laboratory Directed Research and Development program at Los Alamos National Laboratory (LANL) under project 20200073DR. LANL is operated by Triad National Security, LLC, for the National Nuclear Security Administration of U.S. Department of Energy (DOE)(Contract No. 89233218CNA000001). YM is supported from JSPS KAKENHI (15H05815, 15H05747, 16H06286, 20H01959). This study was supported by JSPS Bilateral Open Partnership Joint Research Projects and Grant-in-Aid for Scientific Research (20K14546) of Japan Society for the Promotion of Science (JSPS).

Figure and Table Captions

Figure 1. Locations of RBSPA (red) and Arase (blue) from 0100-0200 UT on August 21, 2017: (a) GSM Y vs GSM X, (b) GSM Z vs GSM Y, and (c) GSM Z vs GSM X.

Figure 2. Overview of geomagnetic conditions and Van Allen Probe A wave observations from 0000-0200 on August 21, 2017. OMNI data from WDC Kyoto of the (a) AE and (b) SYM/H geomagnetic indices; (c) Electric and (d) Magnetic field spectrograms of the wave amplitude from the EMFISIS instrument onboard Van Allen Probe A.

Figure 3. Van Allen Probe EFW Burst Electric (a) and Magnetic (b) Field spectrograms; Arase Electric (c) and Magnetic (d) Field spectrograms of the 5800-7300 Hz burst waveforms from 01:45:17-01:45:47 UT on August 21, 2017.

Figure 4. 5800-7300 Hz Burst Magnetic Field spectrograms from (a) Van Allen Probes A EFW, and (c) Arase from 01:45:36-01:45:46 UT on August 21, 2017; (b) Van Allen Probes and (d) Arase wave normal angles of the magnetic field waveform data from 0-90 degrees; (e) Parallel Poynting flux of the waves observed on Van Allen Probes A, with positive=northward.

Figure 5. Histogram of the WNA calculated at each frequency and time bin shown in Figure 4.

Figure 6. Trajectories of 30 rays with initial position x_0 equally spaced in the $[3.9-4.2]R_E$ interval, initial wave normal angle 18° and 6.8 kHz frequency. The black solid (dashed) line corresponds to the trajectory of the first (last) ray. The red diamond (square) is the position of Van Allen Probes (Arase). The background density model is given by Eq. (1).

Table 1. Ray-tracing simulations data for rays initialized in the equatorial plane and intercepting both spacecraft: x_0 is the range of initial positions of the rays, α_0 is the initial range of wave normal angles, Δt is the range of propagation times between Van Allen Probes and Arase, α_{VAP} (α_{ARASE}) is the wave normal angle at Van Allen Probes (Arase), $|B_{VAP}|/|B_{ARASE}|$ is the ratio of the wave magnetic field amplitude at Van Allen Probes relative to Arase. Both the mean and the min-max range are reported for α_{VAP} , α_{ARASE} and $|B_{VAP}|/|B_{ARASE}|$.

Figure A1. Cold plasma density estimate using the upper hybrid line observed by EMFISIS on Van Allen Probes RBSP-A (symbols), and two models overlaid on the data. Model 1 uses the L^{-4} dependence in Eq. (4) and Model 2 uses the L^{-5} dependence in Eq. (1).

References

Agapitov, O., Artemyev, A., Krasnoselskikh, V., Khotyaintsev, Y. V., Mourenas, D., Breuillard, H., Balikhin, M., & Rolland, G. (2013). Statistics of whistler mode waves in the outer radiation belt: Cluster STAFF-SA measurements. *Journal of Geophysical Research: Space Physics*, 118, 3407– 3420. <https://doi.org/10.1002/jgra.50312>

Agapitov, O. V., Artemyev, A. V., Mourenas, D., Mozer, F. S., & Krasnoselskikh, V. (2015). Empirical model of lower band chorus wave distribution in the outer radiation belt. *Journal of Geophysical Research: Space Physics*, 120, 10,425– 10,442. <https://doi.org/10.1002/2015JA021829>

Agapitov, O., Blum, L. W., Mozer, F. S., Bonnell, J. W., & Wygant, J. (2017). Chorus whistler wave source scales as determined from multipoint Van Allen Probe measurements. *Geophysical Research Letters*, 44, 2634– 2642. <https://doi.org/10.1002/2017GL072701>

Agapitov, O., Mourenas, D., Artemyev, A., Mozer, F. S., Bonnell, J. W., Angelopoulos, V., Shastun, V., & Krasnoselskikh, V. (2018). Spatial extent and temporal correlation of chorus and hiss: Statistical results from multipoint THEMIS observations. *Journal of Geophysical Research: Space Physics*, 123, 8317– 8330. <https://doi.org/10.1029/2018JA025725>

Albert, J. M. (2017), Quasi-linear diffusion coefficients for highly oblique whistler mode waves, *J. Geophys. Res. Space Physics*, 122, 5339–5354, doi:10.1002/ 2017JA024124.

Anderson, K. A., & Milton, D. W. (1964). Balloon observations of X-rays in the auroral zone: 3. High time resolution studies. *Journal of Geophysical Research*, 69(21), 4457–4479. <https://doi.org/10.1029/JZ069i021p04457>

Artemyev, A. V., O. V. Vasiliev, D. Mourenas, V. Krasnoselskikh, V. Shastun, and F. Mozer (2016), Oblique whistler-mode waves in the Earth's inner magnetosphere: Energy distribution, origins, and role in radiation belt dynamics, *Space Sci. Rev.*, 200, 261–355, doi:10.1007/s11214-016-0252-5.

Blake, J. B., Looper, M. D., Baker, D. N., Nakamura, R., Klecker, B., & Hovestadt, D. (1996). New high temporal and spatial resolution measurements by SAMPEX of the precipitation of relativistic electrons. *Advances in Space Research*, 18, 171–186.

Bortnik, J., R. M. Thorne, N. P. Meredith, and O. Santolik (2007a), Ray tracing of penetrating chorus and its implications for the radiation belts, *Geophys. Res. Lett.*, 34, L15109, doi:10.1029/2007GL030040.

Bortnik, J., R. M. Thorne, and N. P. Meredith (2007b), Modeling the propagation and characteristics of chorus using CRRES suprathermal fluxes, *J. Geophys. Res.*, doi:10.1029/2006JA012237.

Bortnik, J., Thorne, R. M., & Meredith, N. P. (2008). The unexpected origin of plasmaspheric hiss from discrete chorus emissions. *Nature*, 452, 62–66. <https://doi.org/10.1038/nature06741>

Bortnik, J., et al. (2009), First observation linking the origin of plasmaspheric hiss to discrete chorus emissions, *Science*, 324, 775– 778, doi:10.1126/science.1171273.

Breneman, A., Kletzing, C. A., Chum, J., Santolik, O., Gurnett, D., & Pickett, J. (2007). Multispacecraft observations of chorus dispersion and source location. *Journal of Geophysical Research*, **112**, A05221. <https://doi.org/10.1029/2006JA012058>

Breneman, A. W., Crew, A., Sample, J., Klumpar, D., Johnson, A., Agapitov, O., et al. (2017). Observations directly linking relativistic electron microbursts to whistler mode chorus: Van Allen Probes and FIREBIRD II. *Geophysical Research Letters*, **44**, 11,265– 11,272. <https://doi.org/10.1002/2017GL075001>

Breuillard, H., Y. Zaliznyak, V. Krasnoselskikh, O. Agapitov, A. Artemyev, and G. Rolland, Chorus wave-normal statistics in the Earth's radiation belts from ray tracing technique, *Ann. Geophys.*, 30, 1223–1233, 2012, www.ann-geophys.net/30/1223/2012/doi:10.5194/angeo-30-1223-2012.

Breuillard, H., Zaliznyak, Y., Agapitov, O., Artemyev, A., Krasnoselskikh, V., and Rolland, G.: Spatial spreading of magnetospherically reflected chorus elements in the inner magnetosphere, *Ann. Geophys.*, 31, 1429–1435, <https://doi.org/10.5194/angeo-31-1429-2013>, 2013.

Burtis, W. J., & Helliwell, R. A. (1969). Banded chorus—A new type of VLF radiation observed in the magnetosphere by OGO 1 and OGO 3. *Journal of Geophysical Research*, **74**, 3002. <https://doi.org/10.1029/JA074i011p03002>

Cattell, C., Wygant, J. R., Goetz, K., Kersten, K., Kellogg, P. J., von Rosenvinge, T.,...Russell, C. T. (2008). Discovery of very large amplitude whistler-mode waves in Earth's radiation belts. *Geophysical Research Letters*, 35, L01105. <https://doi.org/10.1029/2007GL032009>

Cattell, C. A., Breneman, A., Goetz, K., Kellogg, P. J., Kersten, K., Wygant, J. R.,...Roth, I. (2012). Large-amplitude whistler waves and electron acceleration in the Earth's radiation belts: A review of STEREO and Wind observations. In D. Summers et al. (Eds.), *Dynamics of the Earth's Radiation Belts and Inner Magnetosphere* (Vol. 199, pp. 41–51). Washington, DC: American Geophysical Union. <https://doi.org/10.1029/2012GM001322>

Chen, L., Thorne, R. M., Li, W., & Bortnik, J. (2013). Modeling the wave normal distribution of chorus waves. *Journal of Geophysical Research: Space Physics*, 118, 1074–1088. <https://doi.org/10.1029/2012JA018343>

Crew, A. B., et al. (2016), First multipoint in situ observations of electron microbursts: Initial results from the NSF FIREBIRD II mission, *J. Geophys. Res. Space Physics*, 121, doi:10.1002/2016JA022485.

Falkowski, B. J., Tsurutani, B. T., Lakhina, G. S., & Pickett, J. S. (2017). Two sources of dayside intense, quasi-coherent plasmaspheric hiss: A new mechanism for the slot region? *Journal of Geophysical Research: Space Physics*, 122, 1643–1657. <https://doi.org/10.1002/2016JA023289>.

Hanzelka, M., & Santolik, O. (2019). Effects of ducting on whistler mode chorus or exohiss in the outer radiation belt. *Geophysical Research Letters*, 46, 5735-5745. <https://doi.org/10.1029/2019GL083115>

Hartley, D. P., Kletzing, C. A., Santolik, O., Chen, L., & Horne, R. B. (2018). Statistical properties of plasmaspheric hiss from Van Allen Probes observations. *Journal of Geophysical Research: Space Physics*, 123, 2605–2619. <https://doi.org/10.1002/2017JA024593>

Hartley, D. P., Kletzing, C. A., Chen, L., Horne, R. B., & Santolik, O. (2019). Van Allen Probes observations of chorus wave vector orientations: Implications for the chorus-to-hiss mechanism. *Geophysical Research Letters*, 46, 2337–2346. <https://doi.org/10.1029/2019GL082111>

Horne, R. B. (1989), Path-integrated growth of electrostatic waves: The generation of terrestrial myriametric radiation, *J. Geophys. Res.*, 94(A7), 8895– 8909, doi:[10.1029/JA094iA07p08895](https://doi.org/10.1029/JA094iA07p08895).

Horne, R. B., & Thorne, R. M. (1998). Potential waves for relativistic electron scattering and stochastic acceleration during magnetic storms. *Geophysical Research Letters*, 25(15), 3011–3014. <https://doi.org/10.1029/98GL01002>

Horne, R. B., & Thorne, R. M. (2003). Relativistic electron acceleration and precipitation during resonant interactions with whistler-mode chorus. *Geophysical Research Letters*, 30, 1527. <https://doi.org/10.1029/2003GL016973>

Hosokawa, K., Y. Miyoshi, M. Ozaki, S.-I. Oyama, Y. Ogawa, S. Kurita, Y. Kasahara, Y. Kasaba, S. Yagitani, S. Matsuda, F. Tsuchiya, A. Kumamoto, R. Kataoka, K. Shiokawa, T. Raita, E. Turunen, T. Takashima, I. Shinoara and R. Fujii (2020), Multiple time-scale beats in aurora: precise orchestration via magnetospheric chorus waves, *Scientific Reports*, 10, 3380, doi:[10.1038/s41598-020-59642-8](https://doi.org/10.1038/s41598-020-59642-8).

Johnson, A. T., M. Shumko, B. Griffith, D. M. Klumpar, J. Sample, L. Springer, N. Leh, H. E. Spence, S. Smith A. Crew, M. Handley, K. M. Mashburn, B. A. Larsen, J. B. Blake (2020). The FIREBIRD-II CubeSat mission: Focused investigations of relativistic electron burst intensity, range, and dynamics. *Review of Scientific Instruments* **91**, 034503; <https://doi.org/10.1063/1.5137905>

Kasahara, S., Y. Miyoshi, S. Yokota, T. Mitani, Y. Kasahara, S. Matsuda, A. Kumamoto, A. Matsuoka, Y. Kazama, H.U. Frey, V. Anvelopoulos, S. Kurita, K. Keika, K. Seki, and I. Shinohara (2018a), Pulsating aurora from electron scattering by chorus waves, *Nature*, 554, 337-340, doi:[10.1038/nature25505](https://doi.org/10.1038/nature25505).

Kasahara Y, Kasaba Y, Kojima H, Yagitani S, Ishisaka K, Kumamoto A, Tsuchiya F, Ozaki M, Matsuda S, Imachi T, Miyoshi Y, Hikishima M, Katoh Y, Ota M, Shoji M, Matsuoka A, Shinohara I (2018b) The Plasma Wave Experiment (PWE) on board the Arase (ERG) Satellite. *Earth Planets Space*. <https://doi.org/10.1186/s40623-018-0842-4>

Katoh, Y. (2014), A simulation study of the propagation of whistler-mode chorus in the Earth's inner magnetosphere, *Earth Planets Space*, **66**, 6, doi:[10.1186/1880-5981-66-6](https://doi.org/10.1186/1880-5981-66-6).

Kersten, K., Cattell, C. A., Breneman, A., Goetz, K., Kellogg, P. J., Wygant, J. R., Wilson III, L. B., Blake, J. B., Looper, M. D., & Roth, I. (2011). Observation of relativistic electron microbursts in conjunction with intense radiation belt whistler-mode waves. *Geophysical Research Letters*, **38**, L08107.

Kletzing, C., Kurth, W. S., Acuna, M., MacDowall, R. J., Torbert, R. B., Averkamp, T.,... Tyler, J. (2013). The Electric and Magnetic Field Instrument Suite and Integrated Science (EMFISIS) on RBSP. *Space Science Reviews*, 179(1-4), 127–181.
<https://doi.org/10.1007/s11214-013-9993-6>

Kurita, S., Y. Katoh, Y. Omura, V. Angelopoulos, C. M. Cully, O. Le Contel, and H. Misawa (2012), THEMIS observation of chorus elements without a gap at half the gyrofrequency, *J. Geophys. Res.*, **117**, A11223, doi:[10.1029/2012JA018076](https://doi.org/10.1029/2012JA018076)

LeDocq, M. J., D. A. Gurnett, and G. B. Hospodarsky, Chorus source locations from VLF Poynting flux measurements with the Polar spacecraft, *Geophys. Res. Lett.*, **25**, 4063–4066, 1998. Doi: [10.1029/1998GL900071](https://doi.org/10.1029/1998GL900071)

Li, W., Thorne, R. M., Angelopoulos, V., Bortnik, J., Cully, C. M., Ni, B.,... Magnes, W. (2009). Global distribution of whistler-mode chorus waves observed on the THEMIS spacecraft. *Geophysical Research Letters*, 36, L09104. <https://doi.org/10.1029/2009GL037595>

Li, W., Bortnik, J., Thorne, R. M., & Angelopoulos, V. (2011). Global distribution of wave amplitudes and wave normal angles of chorus waves using THEMIS wave observations. *Journal of Geophysical Research*, 116(A12), A12205. <https://doi.org/10.1029/2011JA017035>

Li, W., Bortnik, J., Thorne, R. M., Cully, C. M., Chen, L., Angelopoulos, V., ... LeContel, O. (2013). Characteristics of the Poynting flux and wave normal vectors of whistler-mode waves observed on THEMIS. *Journal of Geophysical Research: Space Physics*, 118, 1461–1471. <https://doi.org/10.1002/jgra.50176>

Li, W., Santolik, O., Bortnik, J., Thorne, R. M., Kletzing, C. A., Kurth, W. S., & Hospodarsky, G. B. (2016). New chorus wave properties near the equator from Van Allen Probes wave observations. *Geophysical Research Letters*, 43, 4725–4735. <https://doi.org/10.1002/2016GL068780>

Lorentzen, K. R., Looper, M. D., & Blake, J. B. (2001a). Relativistic electron microbursts during the GEM storms. *Geophysical Research Letters*, 28(13), 2573–2576. <https://doi.org/10.1029/2001GL012926>

Lorentzen, K. R., Blake, J. B., Inan, U. S., & Bortnik, J. (2001b). Observations of relativistic electron microbursts in association with VLF chorus. *Journal of Geophysical Research*, 106(A4), 6017–6027. <https://doi.org/10.1029/2000JA003018>

Malaspina, D. M., Jaynes, A. N., Boulé, C., Bortnik, J., Thaller, S. A., Ergun, R. E., Kletzing, C. A., & Wygant, J. R. (2016). The distribution of plasmaspheric hiss wave power with respect to plasmopause location. *Geophysical Research Letters*, 43, 7878–7886. <https://doi.org/10.1002/2016GL069982>

Malaspina, D. M., Ripoll, J.-F., Chu, X., Hospodarsky, G., & Wygant, J. (2018). Variation in plasmaspheric hiss wave power with plasma density. *Geophysical Research Letters*, 45, 9417–9426. <https://doi.org/10.1029/2018GL078564>

Matsuda, S., Y. Kasahara, H. Kojima, Y. Kasaba, S. Yagitani, M. Ozaki, T. Imachi, K. Ishisaka, A. Kumamoto, F. Tsuchiya, M. Ota, S. Kurita, Y. Miyoshi, M. Hikishima, A. Matsuoka, and I. Shinohara (2018), Onboard Software of Plasma Wave Experiment aboard Arase: Instrument Management and Signal Processing of Waveform Capture/Onboard Frequency Analyzer, *Earth, Planets and Space*, 70:75, doi:10.1186/s40623-018-0838-0.

Matsuoka, A., M. Teramoto, R. Nomura, M. Nosé, A. Fujimoto, Y. Tanaka, M. Shinohara, T. Nagatsuma, K. Shiokawa, Y. Obana, Y. Miyoshi, M. Mita, T. Takashima, and I. Shinohara (2018), The ARASE(ERG) magnetic field investigation, *Earth, Planets and Space*, 70, 43, 10.1186/s40623-018-0800-1.

Means, J. D. (1972) , Use of the three-dimensional covariance matrix in analyzing the polarization properties of plane waves, *J. Geophys. Res.*, **28**, 5551, doi:10.1029/JA077i028p05551.

Meredith, N. P., Cain, M., Horne, R. B., Thorne, R. M., Summers, D., & Anderson, R. R. (2003). Evidence for chorus-driven electron acceleration to relativistic energies from a survey of geomagnetically disturbed periods. *Journal of Geophysical Research*, 108(A6), 1248. <https://doi.org/10.1029/2002JA009764>

Meredith, N. P., Horne, R. B., Clilverd, M. A., Horsfall, D., Thorne, R. M., & Anderson, R. R. (2006). Origins of plasmaspheric hiss. *Journal of Geophysical Research*, 111(A9), A09217. <https://doi.org/10.1029/2006JA011707>

Meredith, N. P., Horne, R. B., Bortnik, J., Thorne, R. M., Chen, L., Li, W., & Sicard-Piet, A. (2013). Global statistical evidence for chorus as the embryonic source of plasmaspheric hiss. *Geophysical Research Letters*, 40, 2891–2896. <https://doi.org/10.1002/grl.50593>

Miyoshi, Y., A. Morioka, T. Obara, H. Misawa, T. Nagai, and Y. Kasahara (2003), Rebuilding process of the outer radiation belt during the November 3, 1993, magnetic storm - NOAA and EXOS-D observations, *J. Geophys. Res.* , 108(A1), 1004, doi:10.1029/2001JA007542.

Miyoshi, Y., S. Saito, K. Seki, T. Nishiyama, R. Kataoka, K. Asamura, Y. Katoh, Y. Ebihara, T. Sakanoi, M. Hirahara, S. Oyama, S. Kurita, and O. Santolik (2015a), Relation between energy spectra of pulsating aurora electrons and frequency spectra of whistler-mode chorus waves, *J. Geophys. Res.*, 120, 7728-7736, doi:10.1002/2015JA021562.

Miyoshi, Y., S. Oyama, S. Saito, H. Fujiwara, R. Kataoka, Y. Ebihara, C. Kletzing, G. Reeves, O. Santolik, M. Cliverd, C. Rodger, E. Turunen, and F. Tsuchiya (2015b), Energetic electron precipitation associated with pulsating aurora: EISCAT and Van Allen Probes observations, *J. Geophys. Res.*, 120, doi:10.1002/2014JA020690.

Miyoshi Y, Shinohara I, Takashima T, Asamura K, Higashio N, Mitani T, Kasahara S, Yokota S, Kazama Y, Wang S-Y, Tam SW, Ho, P.T.P, Kasahara, Y, Kasaba Y, Yagitani S, Matsuoka A, Kojima H, Katoh H, Shiokawa K, Seki K (2018a), Geospace Exploration Project ERG, *Earth Planets Space*, 70:101, doi:10.1186/s40623-018-0862-0.

Miyoshi Y, Hori T, Shoji M, Teramoto M, Chang T-F, Segawa T, Umemura N, Matsuda S, Kurita S, Keika K, Miyashita Y, Seki K, Tanaka Y, Nishitani N, Kasahara S, Yokota S, Matsuoka A, Kasahara Y, Asamura K, Takashima T, Shinohara I (2018b), The ERG science center. *Earth Planets Space* 70:96. <https://doi.org/10.1186/s40623-018-0867-8>

Mozer, F. S., Agapitov, O. V., Blake, J. B., & Vasko, I. Y. (2018). Simultaneous observations of lower band chorus emissions at the equator and microburst precipitating electrons in the ionosphere. *Geophysical Research Letters*, **45**, 511– 516. <https://doi.org/10.1002/2017GL076120>

Nakamura, R., Isowa, M., Kamide, Y., Baker, D. N., Blake, J. B., & Looper, M. (2000). SAMPEX observations of precipitation bursts in the outer radiation belt. *Journal of Geophysical Research*, 105, 15,875–15,886. <https://doi.org/10.1029/2000JA900018>

Nishimura, Y., Bortnik, J., Li, W., Thorne, R. M., Lyons, L. R., Angelopoulos, V., ... Auster, U. (2010). Identifying the driver of pulsating aurora. *Science*, 330(6000), 81–84. <https://doi.org/10.1126/science.1193186>

O'Brien, T. P., Looper, M. D., & Blake, J. B. (2004). Quantification of relativistic electron microburst losses during the geom storms. *Geophysical Research Letters*, *31*, L04802. <https://doi.org/10.1029/2003GL018621>

Oliven, M. N., & Gurnett, D. A. (1968). Microburst phenomena: 3. An association between microbursts and VLF chorus. *Journal of Geophysical Research*, *73*, 2355–2362. <https://doi.org/10.1029/JA073i007p02355>

Omura, Y., Katoh, Y., & Summers, D. (2008). Theory and simulation of the generation of whistler-mode chorus. *Journal of Geophysical Research*, *113*(A4), A04223. <https://doi.org/10.1029/2007JA012622>

Ozaki, M., Y. Miyoshi, K. Shiokawa, K. Hosokawa, S. Oyama, R. Kataoka, Y. Ebihara, Y. Ogawa, Y. Kasahara, S. Yagitani, Y. Kasaba, A. Kumamoto, F. Tsuchiya, S. Matsuda, Y. Katoh, M. Hikishima, S. Kurita, R. Moore, Y. Takanaka, M. Nose, T. Nagatsuma, N. Nishitani, A. Kadokura, M. Connors, A. Matsuoka, and I. Shinohara (2019), Visualization of rapid electron precipitation via chorus element wave–particle interactions, *Nature Comm*, *10*, 257, doi:10.1038/s41467-018-07996-z.

Reeves, G. D., Spence, H. E., Henderson, M. G., Morley, S. K., Friedel, R. H. W., Funsten, H. O.,...Niehof, J. T. (2013). Electron acceleration in the heart of the Van Allen radiation belts. *Science*, 341(6149), 991–994. <https://doi.org/10.1126/science.1237743>

Ripoll, J. - F., Claudepierre, S. G., Ukhorskiy, A. Y., Colpitts, C., Li, X., Fennell, J., & Crabtree, C. (2020). Particle Dynamics in the Earth's Radiation Belts: Review of Current Research and Open Questions. *Journal of Geophysical Research: Space Physics*, 125, e2019JA026735. <https://doi.org/10.1029/2019JA026735>

Rosenberg, T. J., Helliwell, R. A., & Katsufakis, J. P. (1971). Electron precipitation associated with discrete very-low-frequency emissions. *Journal of Geophysical Research*, 76(34), 8445–8452. <https://doi.org/10.1029/JA076i034p08445>

Rosenberg, T. J., Siren, J. C., Matthews, D. L., Marthinsen, K., Holtet, J. A., Egeland, A.,...Helliwell, R. A. (1981). Conjugacy of electron microbursts and VLF chorus. *Journal of Geophysical Research*, 86(A7), 5819–5832. <https://doi.org/10.1029/JA086iA07p05819>

Santolík, O., Parrot, M., and Lefeuvre, F. (2003), Singular value decomposition methods for wave propagation analysis, *Radio Sci.*, 38, 1010, doi:10.1029/2000RS002523, 1.

Santolik, O., Chum, J., Parrot, M., Gurnett, D. A., Pickett, J. S., & Cornilleau-Wehrin, N. (2006). Propagation of whistler mode chorus to low altitudes: Spacecraft observations of structured ELF hiss. *Journal of Geophysical Research*, 111(A10), A10208. <https://doi.org/10.1029/2005JA011462>

Santolik, O., Gurnett, D. A., Pickett, J. S., Chum, J., & Cornilleau-Wehrin, N. (2009). Oblique propagation of whistler mode waves in the chorus source region. *Journal of Geophysical Research*, 114(A12), A00F03. <https://doi.org/10.1029/2009JA014586>

Santolik, O., Pickett, J. S., Gurnett, D. A., Menietti, J. D., Tsurutani, B. T., & Verkhoglyadova, O. (2010). Survey of Poynting flux of whistler mode chorus in the outer zone. *Journal of Geophysical Research*, 115(A7), A00F13. <https://doi.org/10.1029/2009JA014925>

Santolik, O., Kletzing, C. A., Kurth, W. S., Hospodarsky, G. B., & Bounds, S. R. (2014). Fine structure of large-amplitude chorus wave packets. *Geophysical Research Letters*, 41, 293–299. <https://doi.org/10.1002/2013GL058889>

Sheeley, B. W., M. B. Moldwin, H. K. Rassoul, and R. R. Anderson (2001), An empirical plasmasphere and trough density model: CRRES observations, *J. Geophys. Res.*, 106, 25,631.

Spence, H. E., Blake, J. B., Crew, A. B., Driscoll, S., Klumpar, D. M., Larsen, B. A.,...Widholm, M. (2012). Focusing on size and energy dependence of electron microbursts from the Van Allen radiation belts. *Space Weather*, 10, S11004. <https://doi.org/10.1029/2012SW000869>

Summers, D., B. Ni, and N. P. Meredith (2007), Timescales for radiation belt electron acceleration and loss due to resonant wave-particle interactions: 1. Theory, *J. Geophys. Res.*, 112, A04206, doi:10.1029/2006JA011801.

Taylor, W. W. L., & Gurnett, D. A. (1968). Morphology of VLF emissions observed with the Injun 3 satellite. *Journal of Geophysical Research*, 73(17), 5615–5626. <https://doi.org/10.1029/JA073i017p05615>

Thorne, R. M., Smith, E. J., Burton, R. K., & Holzer, R. E. (1973). Plasmaspheric hiss. *Journal of Geophysical Research*, 78(10), 1581–1596. <https://doi.org/10.1029/JA078i010p01581>

Thorne, R. M., Ni, B., Tao, X., Horne, R. B., & Meredith, N. P. (2010). Scattering by chorus waves as the dominant cause of diffuse auroral precipitation. *Nature*, 467(7318), 943–946. <https://doi.org/10.1038/nature09467>

Thorne, R. M., Li, W., Ni, B., Ma, Q., Bortnik, J., Chen, L., ... Kanekal, S. G. (2013). Rapid acceleration of relativistic radiation belt electrons by magnetospheric chorus. *Nature*, 504(7480), 411–414. <https://doi.org/10.1038/nature12889>

Tsurutani, B. T., & Smith, E. J. (1977). Two types of magnetospheric ELF chorus and their substorm dependences. *Journal of Geophysical Research*, 82(32), 5112–5128. <https://doi.org/10.1029/JA082i032p05112>

Turner, D. L., Lee, J. H., Claudepierre, S. G., Fennell, J. F., Blake, J. B., Jaynes, A. N., ... Santolik, O. (2017). Examining coherency scales, substructure, and propagation of whistler mode chorus elements with Magnetospheric Multiscale (MMS). *Journal of Geophysical Research: Space Physics*, 122. <https://doi.org/10.1002/2017JA024474>

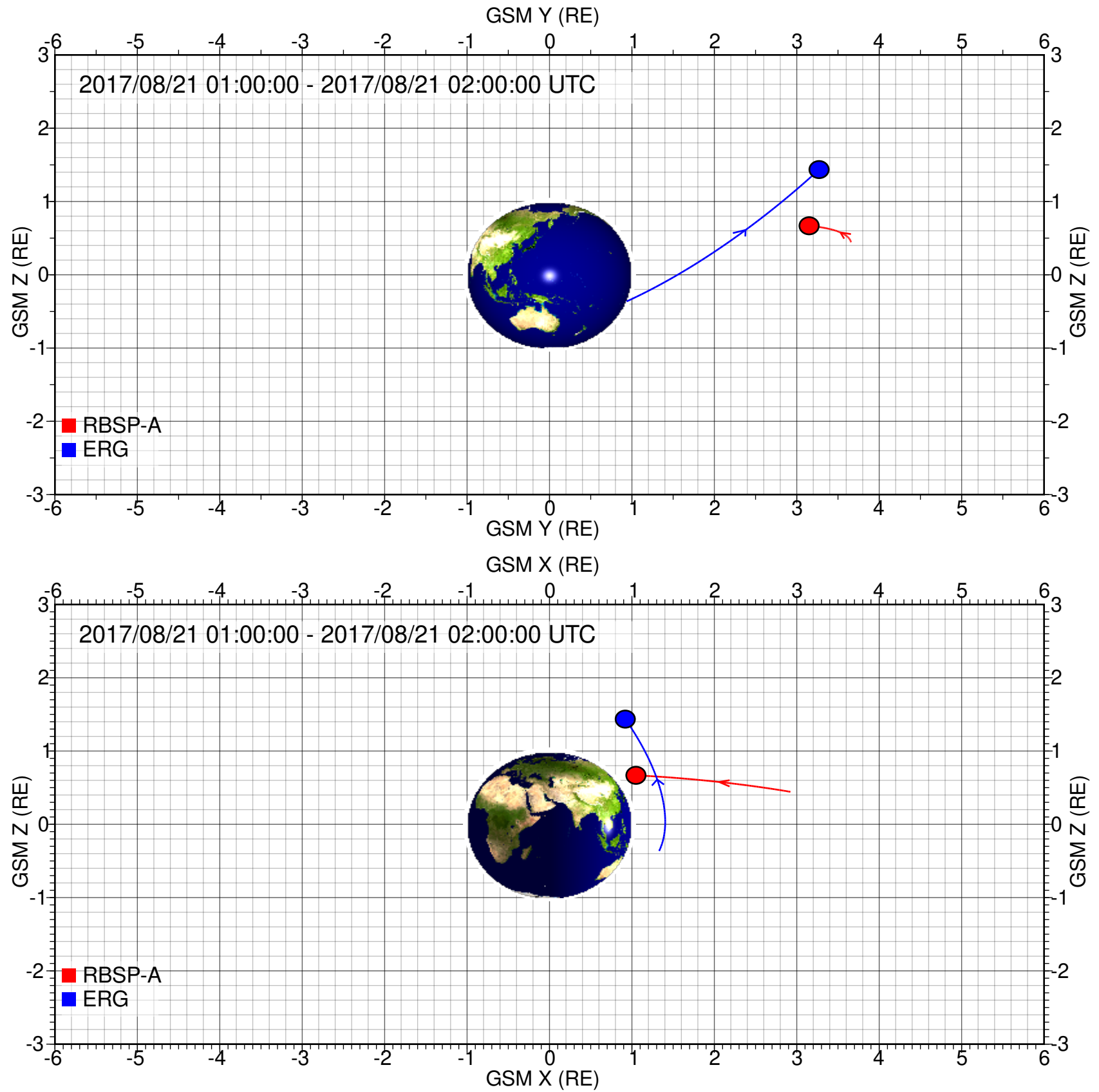
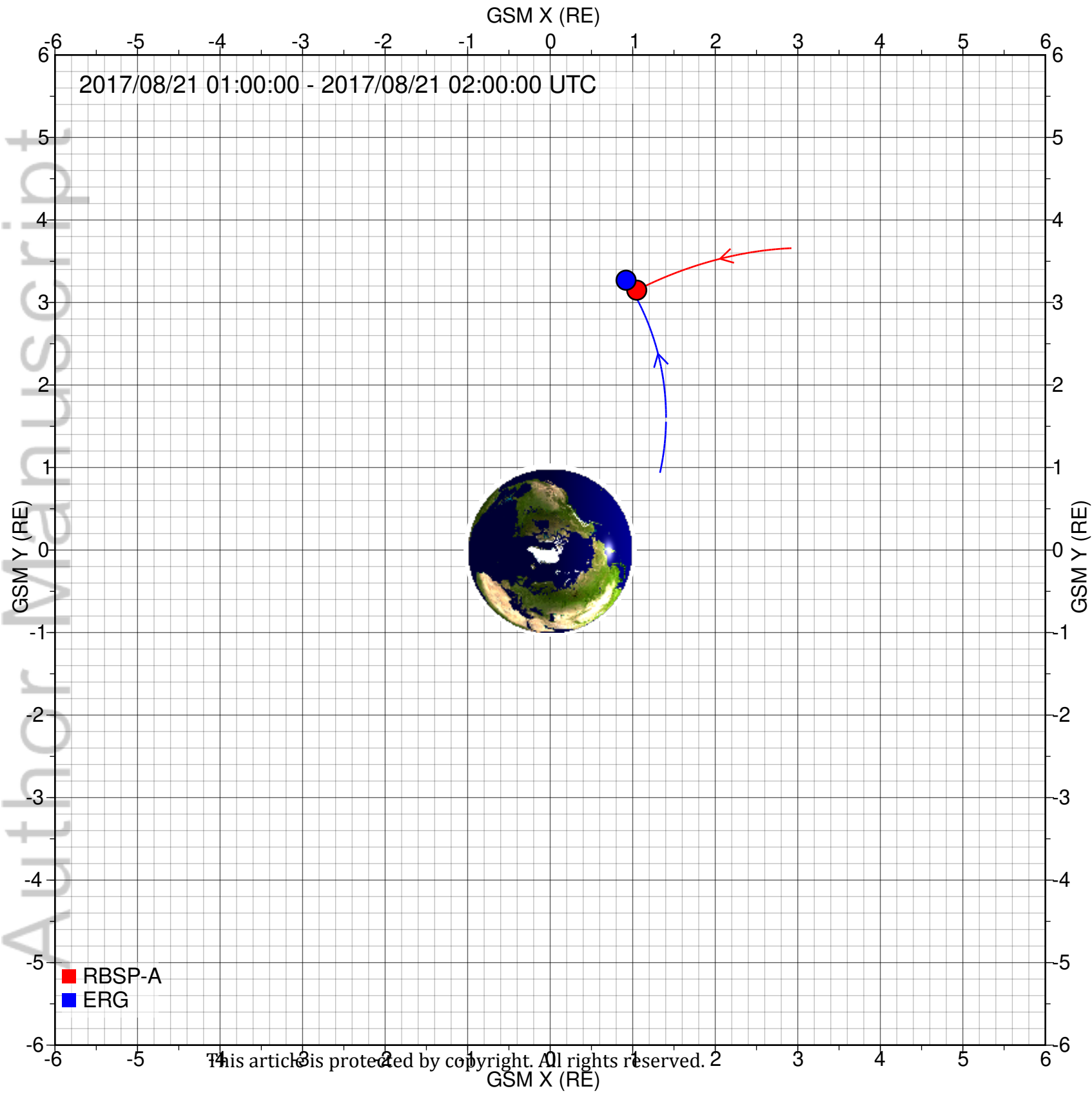
Tyler, E., A. Breneman, C. Cattell, J. Wygant, S. Thaller and D. Malaspina, Statistical Occurrence and Distribution of High-Amplitude Whistler Mode Waves in the Outer Radiation Belt (2019a), *Geophysical Research Letters*, **46**, 5, (2328-2336).

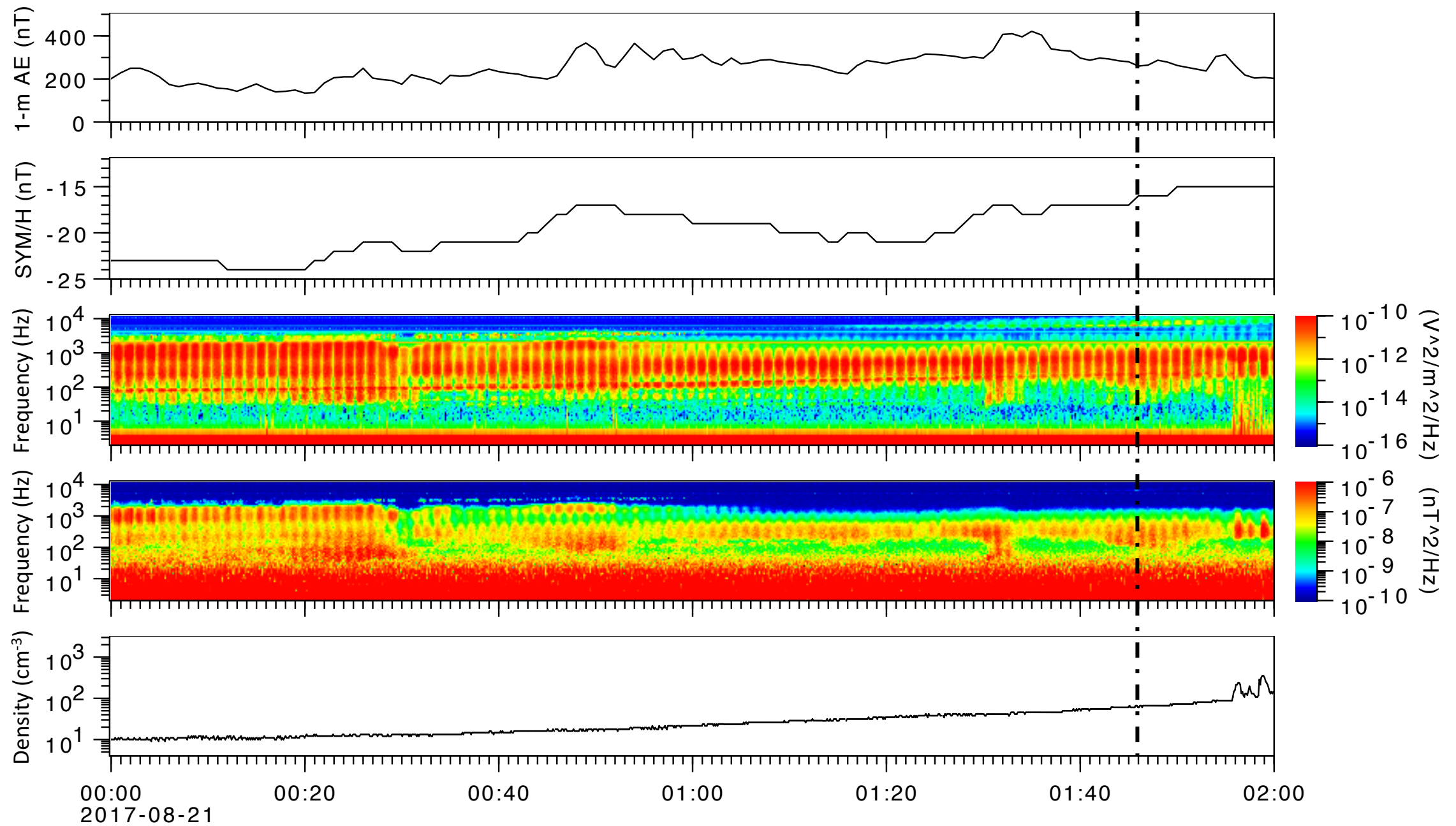
Tyler, E., A. Breneman, C. Cattell, J. Wygant, S. Thaller and D. Malaspina, Statistical Distribution of Whistler Mode Waves in the Radiation Belts With Large Magnetic Field Amplitudes and Comparison to Large Electric Field Amplitudes (2019b), *Journal of Geophysical Research: Space Physics*, **124**, 8, (6541-6552)

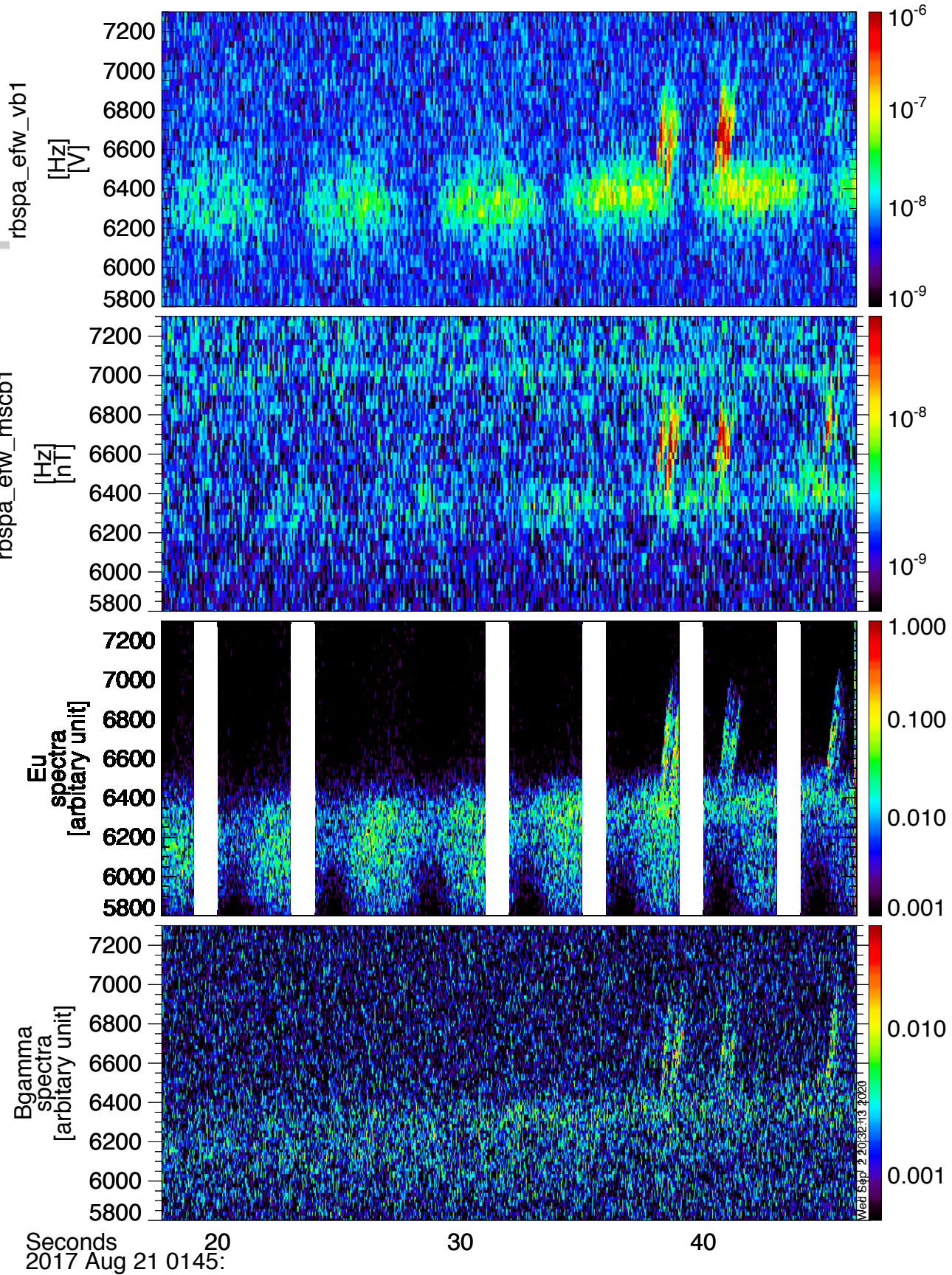
Wygant, J. R., et al. (2013), The electric field and waves instruments on the Radiation Belt Storm Probes mission, *Space Sci. Rev.*, **179**(1–4), 183– 220, doi:[10.1007/s11214-013-0013-7](https://doi.org/10.1007/s11214-013-0013-7).

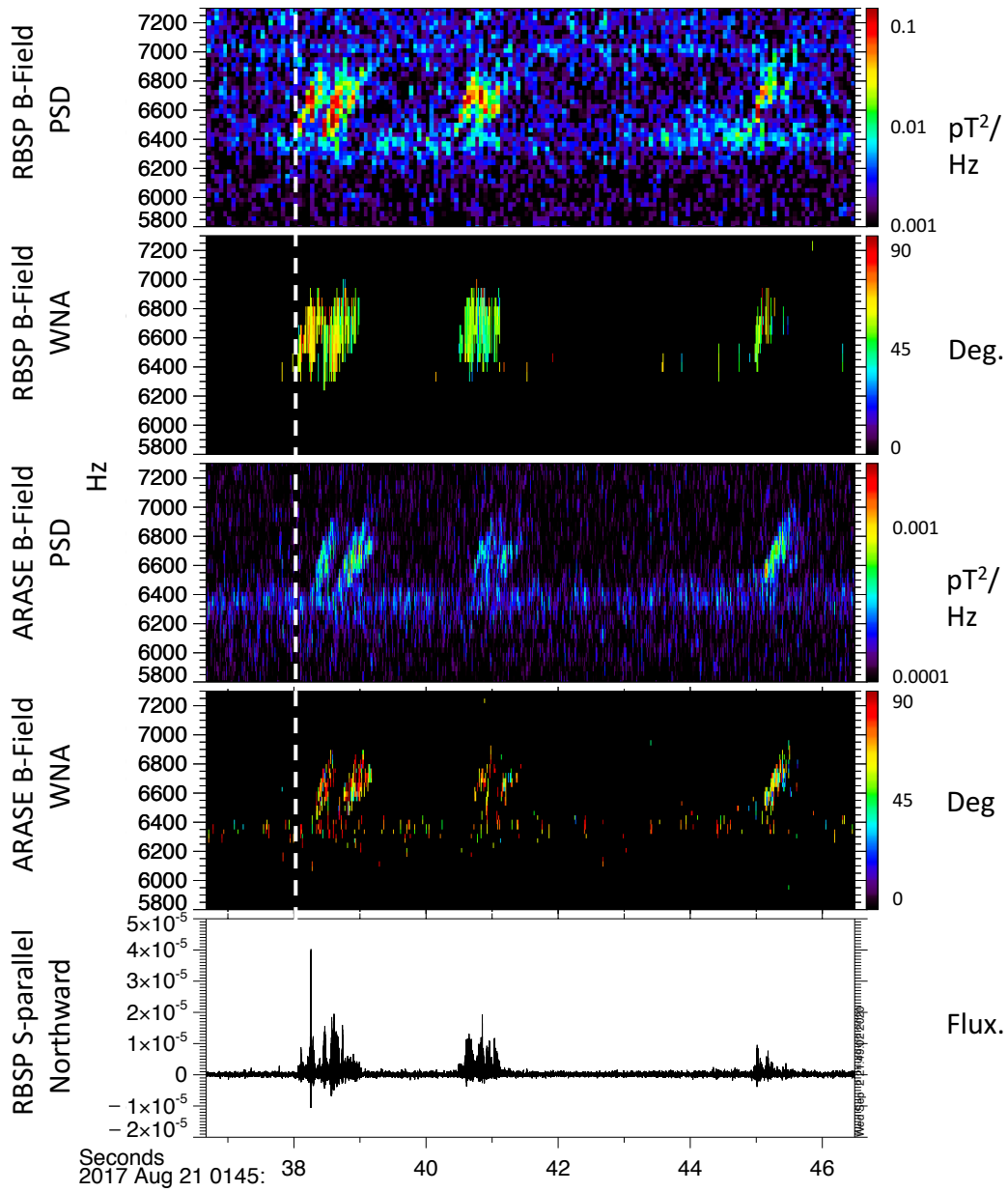
Yearby, K. H., M. A. Balikhin, Y. V. Khotyaintsev, S. N. Walker, V. V. Krasnoselskikh, H. S. C. K. Alleyne, and O. Agapitov (2011), Ducted propagation of chorus waves: Cluster observations, *Ann. Geophys.*, **29**, 1629– 1634, doi:[10.5194/angeo-29-1629-2011](https://doi.org/10.5194/angeo-29-1629-2011).

Quantity	f=6.5 kHz $\delta = 0.002$ Eq. (1)	f=6.5 kHz $\delta = 0.005$ Eq. (1)	f=6.5 kHz $\delta = 0.01$ Eq. (1)	f=6.8 kHz $\delta = 0.005$ Eq. (1)	f=7.1 kHz $\delta = 0.005$ Eq. (1)	f=6.8 kHz $\delta = 0.005$ Eq. (4)
$x_0 [R_E]$	4.00	3.98-4.02	3.94-4.09	3.97-4.02	3.97-4.01	3.95-4.01
$\alpha_0 [^\circ]$	23	22-25	20-27	17-19	12-14	12-15
$\Delta t [s]$	0.132	0.130-0.136	0.127-0.142	0.129-0.133	0.128-0.131	0.128-0.133
$\alpha_{VAP} [^\circ]$ mean	56.8	57.1	57.1	54.4	52.0	53.9
$\alpha_{VAP} [^\circ]$ min-max	56.8	55.8-58.5	53.6-60.2	53.2-55.6	50.8-53.2	52.5-55.8
$\alpha_{ARASE} [^\circ]$ mean	73.1	73.2	73.2	72.1	71.0	72.2
$\alpha_{ARASE} [^\circ]$ min-max	73.1	72.8-73.6	72.1-74.2	71.7-72.4	70.6-71.4	71.9-72.7
$ B_{VAP} / B_{ARASE} $ mean	1.91	1.88	1.89	1.99	2.05	2.22
$ B_{VAP} / B_{ARASE} $ min-max	1.91	1.74-2.03	1.60-2.40	1.85-2.15	1.92-2.20	1.95-2.46

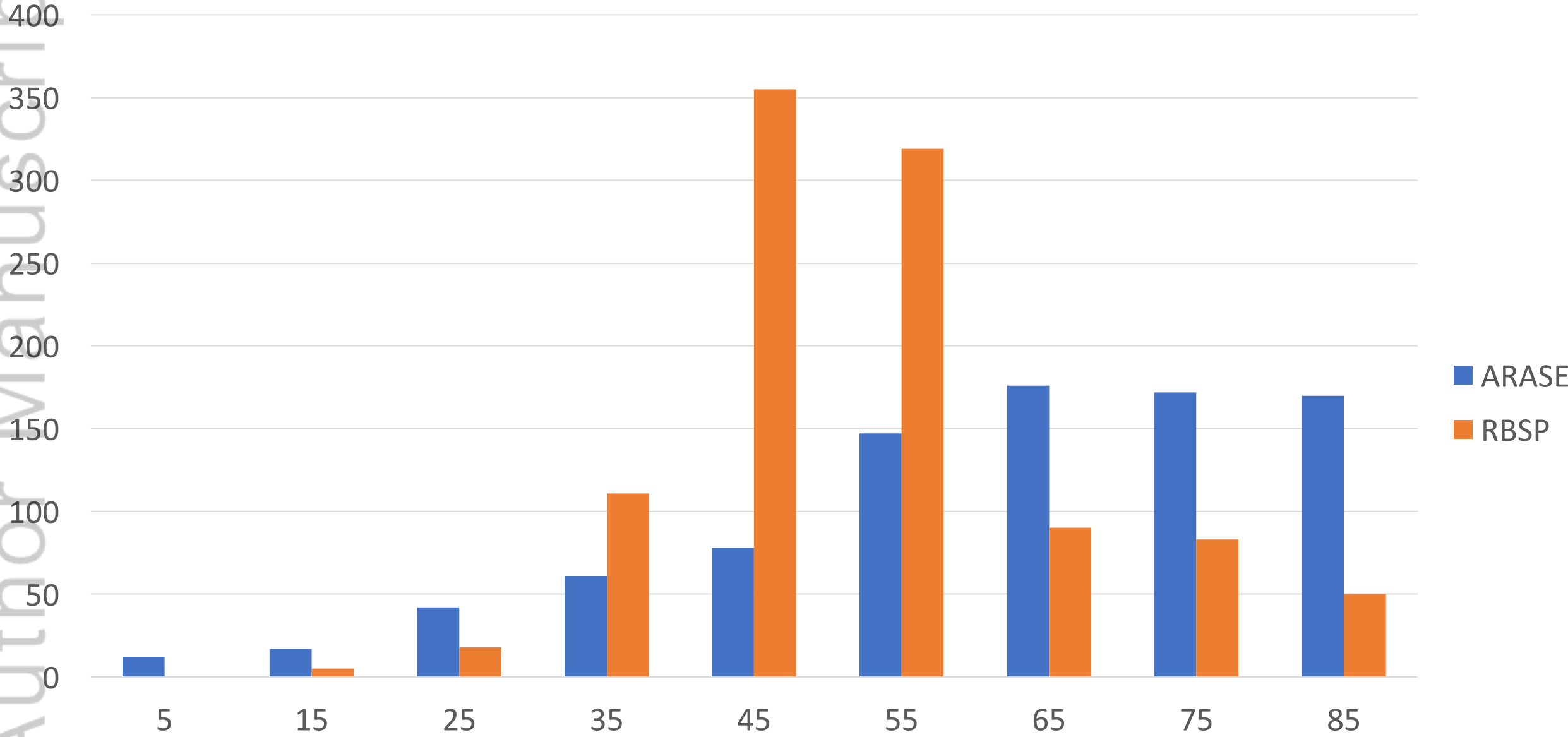




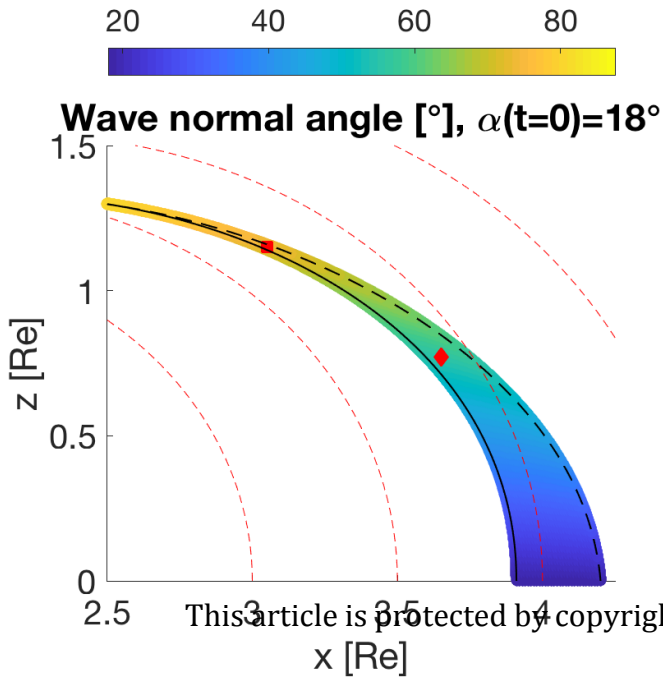




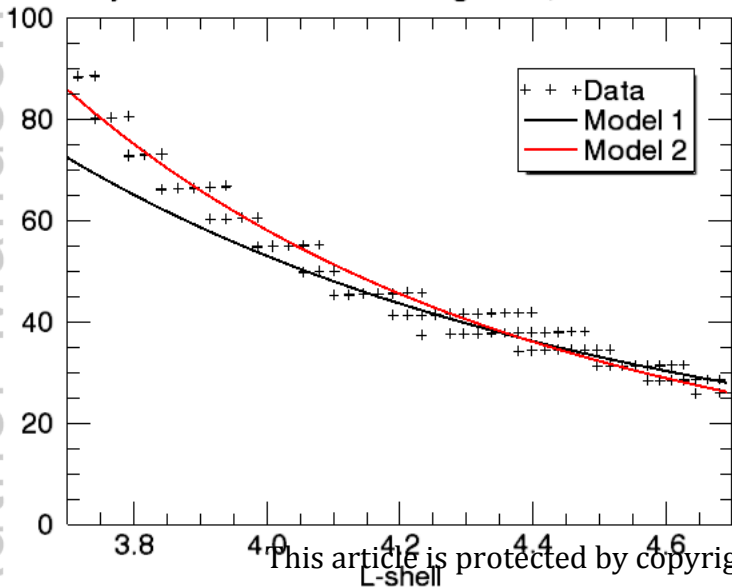
Wave Normal Angle of every data point in 3 chorus elements



Author Manuscript



Density from UHR on RBSP-A August 21, 2017 ~0145 UT



This article is protected by copyright. A